A 500-ps Molecular Dynamics Simulation Trajectory of Cardiotoxin II from Taiwan Cobra Venom in Solution: Correlation with NMR and X-Ray Crystallography Data

YING-CHIEH SUN, SHU-FEN YANG, I-LUNG HWANG, TZU-HSIEN WU

Department of Chemistry, National Taiwan Normal University, 88, Tingchow Road Sec. 4, Taipei 11718, Taiwan, ROC

Received 19 May 1998; revised 9 November 1998; accepted 17 November 1998

ABSTRACT: Molecular dynamics simulation of a small, basic, all β-sheet cardiotoxin, CTX II, from Taiwan cobra venom, with proper treatment of long-range electrostatic interactions, was carried out to examine the backbone mobility of CTX II in solution and aid in interpretation of order parameters of C_α—H bonds obtained from NMR experiments based on the Lipari–Szabo theory. The calculated order parameters of C_α—H bonds and B-factors of CTX II in solution were compared with NMR-derived backbone order parameters and the crystal structure data, respectively. An overall qualitative agreement was obtained and, quantitatively, the calculated values and experimental results of many residues were also in good agreement. The discrepancies between the results computed herein and the experimental values, physical bases, and plausible biological functions are discussed. © 1999 John Wiley & Sons, Inc. J Comput Chem 20: 546–562, 1999

Keywords: protein simulation; cardiotoxin; backbone dynamics; order parameters; B-factors

Correspondence to: Ying-Chieh Sun; e-mail: sun@scc.ntnu.edu.tw

Contract/grant sponsor: National Science Council

CCC 0192-8651 / 99 / 050546-17

Introduction

The cardiotoxins (CTX) I–V from Taiwan cobra venom are small five-β-strand and three-loop basic proteins of 60–62 residues (Fig. 1) that induce contraction and paralysis of frog heart and rat atrial muscle.[1] The primary structure of these cardiotoxins reveals a 70–90% sequence homology[1]; however, significant variations in the biological activity of CTXs in inducing fusion and lysis of synthetic vesicles, depolarization of membranes, etc., are observed.[2–7] In all these proteins, the polypeptide chains are cross-linked by four disulfide bonds that are conserved[8–10] and hold the polypeptide strands together at the top of the molecules. The five β-strands consist of two anti-β-sheets in molecule forming a relatively flat shape, and are connected by three loop segments as shown in Figure 1.[1] The structures of all these proteins were determined by using NMR experiments,[1,11–19] whereas the crystal structure of CTX V was resolved using X-ray crystallography.[20] In addition, important experiments were carried out to investigate the folding/unfolding pathway and the stability of CTXs.[21–28] Moreover, mutation experiments were also carried out to understand the role of residues in the toxicity of CTXs.[29–32] Much progress has been made in understanding the biological action of CTXs, with a focus on interactions between CTXs and membrane.[5,33–36] The various binding modes of CTXs with lipid and saccharide molecules in membrane were also investigated and correlated with their biological activities.[5,33–36] Besides these examinations, attention has been raised in the investigation of binding of CTXs with adenosine triphosphate (ATP).[37] The binding mode and structure of the CTX II–dATP complex were resolved in a recent NMR experiment.[37]

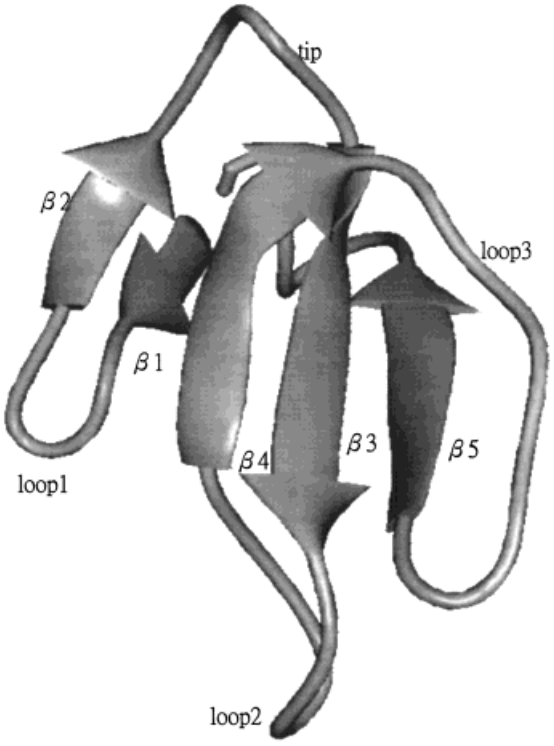

FIGURE 1. Secondary structures of CTX II from Taiwan cobra venom.

Advances in NMR dynamical experiments have permitted examination of the backbone dynamics of biomolecules in solution.[38–51] Based on the Lipari–Szabo model-free theory,[52–55] an order parameter of a fractional number for each observed dynamical NOESY result of a C_α—H or N—H bond of a residue can be derived, which represents the backbone mobility of that residue.[52,53,56,57] The backbone dynamics of a number of proteins have been investigated using this method and the backbone mobility of many residues of these proteins in solution have also been examined.[38–41,43–51] Theoretically, NMR relaxation parameters in molecules have been examined using various approaches.[52,53,56–64] Various molecular dynamics (MD) simulations of proteins have been carried out to examine atomic fluctuation in solution.[65,57,66–68] Based on the model-free formalism,[52,53,56,57] the order parameters using molecular dynamics simulation can be calculated. The calculated order parameters of C_α—H or N—H bonds for residues of proteins have been aided in interpretation of experimental results for structure fluctuation and were correlated with their biological activities.[57,65–68] In addition to order parameters, B-factors, which represent the backbone mobility in the translational degree of freedom, were also calculated to correlate with the temperature factor obtained from X-ray crystallography experiments.[57,65–68] Recently, NMR NOESY dynamical experiments were carried out to investigate the backbone dynamics of one of the small, basic, all β-sheet cardiotoxins, CTX II, in solution of pH 3.[69] The backbone dynamics of this protein were explored in depth, based on the observed dynamical NMR data and five spectral density models. The backbone mobility of 50 residues,

which had order parameters of C_α—H bonds that were already determined, was examined, and their correlations with biological activities have been discussed.[69]

In the present study, MD simulation of CTX II in an explicit water model was carried out to examine the backbone mobility of CTX II. In the simulation, the particle-meshed Ewald (PME) sun method[70] was employed, which was developed recently to describe the long-range electrostatic interactions more accurately than the standard 8-Å cutoff method, and shown to be crucial in the stabilization of protein structures in solution.[70] Using this treatment in MD simulation to examine backbone dynamics of a small protein, ubiquitin, in solution was carried out recently by Fox and Kollman, based on the calculated correlation functions.[71] The calculated results of order parameters were in good agreement with experimental results.[72] In the present study, our aim is to examine the reproducibility of backbone mobility for a small, positively charged, all β-sheet protein (CTX II) using MD simulation with a treatment of long-range electrostatic interactions in an explicit water model, with formulation of eq. (4) (see Method section) for calculating order parameters. The computation is shown to give an overall qualitative agreement between calculated and experimental order parameters of residues in proteins, and the results are aided for interpretation of NMR-derived order parameters.[69] The structure of CTX II in solution is stable throughout the course of MD simulation. The calculated results of C_α—H and N—H reorientation order parameters and B-factors of atomic fluctuation for backbone flexibility are described in the Results and Discussion section, and are compared with experimental results.[20] The reasons for the discrepancies between the calculated and experimental results are also examined. Furthermore, the physical basis for backbone mobility, atomic fluctuation, and the plausible implication of biological function due to actions of CTX II are investigated in terms of molecular interactions, conformations, and structural fluctuation of CTX II.

Method

LIPARI–SZABO MODEL-FREE THEORY

The physical quantities in backbone fluctuation calculated in the present study are described briefly in what follows. Based on the formalism of the Lipari–Szabo model-free theory described in the literature,[52,53,56,57] the correlation function for the internal motion of a bond of interest is defined as[52,53,56,57]:

$$C(t) = \langle r^{-6}(t)\rangle^{-1} \left\langle \frac{P_2[\cos(\chi(t))]}{r^3(0)r^3(t)} \right\rangle \quad (1)$$

where r is the distance between two measured nuclear spins, and $\chi(t)$ is the angle between the internuclear vectors of these two nuclei at time 0 and t, respectively. In eq. (1), $P_2(x)$ is a second-rder Legendre polynomial, $P_2(x) = 1/2(3x^2 - 1)$. In cases where the internal motion can be described by a Markovian process, the time correlation function of the internal motion can be expressed as the sum of a series of exponentials:

$$C_{\text{int}}(t) = \sum_{i=0}^{N} a_i e^{-t/\tau_i} \quad (2)$$

where τ_i represents correlation times, and a_i are their corresponding coefficients. In both limits of $t = 0$ and $t = \infty$, the internal correlation function, C_{int}, can be rendered and approximated by:

$$C_{\text{int}}(t) = S^2 + (1 - S^2)e^{-t/\tau_{\text{int}}} \quad (3)$$

where S^2 is the order parameter defined by:

$$S^2 = \lim_{t\to\infty} C_{\text{int}}(t) = \frac{4\pi}{5}\langle r^{-6}\rangle^{-1} \sum_{m=-2}^{2} \left| \left\langle \frac{Y_{2m}(\theta,\phi)}{r^3} \right\rangle \right|^2 \quad (4)$$

$Y_{2m}(\theta, \phi)$ are the second-order spherical harmonics as functions of the angular spherical coordinates of the internuclear vector in the molecular-fixed frame. The bracketed data represent the statistical ensemble average calculated from the trajectory of MD simulation. The fractional value of order parameter S^2 is a measure of the degree of internal motion freedom of the vector connecting two nuclear spins of interest. In a completely rigid case, the order parameter is equal to 1. Alternately, for the case of a free vector rotor, S^2 is equal to 0. The correlation time, τ_{int}, for internal motion in eq. (3) is calculated according to:

$$\tau_{\text{int}} = \frac{1}{C_{\text{int}}(0) - S^2} \int_0^T dt(C_{\text{int}}(t) - S^2) \quad (5)$$

The errors in the above statistical quantities were calculated using jackknife method[57,73] described elsewhere.[57] For the correlation time of internal

motion, the calculated values are not listed when errors are larger than their correlation time values. In addition to examination of the rotational motion of C_α—H and N—H bonds, the B-factors of backbone heavy atoms for atomic fluctuation in the translational degree of freedom in the MD trajectory were calculated according to[74]:

$$B_i = \frac{8\pi^2}{3}\langle \Delta r_i^2 \rangle \quad (6)$$

where $\langle \Delta r_i^2 \rangle$ is the mean square displacement for the ith atom calculated from the MD trajectory.

SIMULATION

The structure of CTX II was obtained from the NMR solution structure in the PDB databank entry pdb1cre.ent.[16] The charge states of ionizable residues were set to correspond to pH 3.0, at which point the NMR experiments were carried out.[16] Lys and Arg were treated as positively charged residues, whereas Glu and Asp were treated as neutral residues. The ten charged residues, the protonated amino group at the N-terminus, and deprotonated carboxyl group at the C-terminus were neutralized by placing 11 chlorine ions and 1 sodium ion close to the sidechains of the 10 charged residues, and the N- and C-termini, respectively. The energy of this system was then minimized and the system was then solvated in a large box containing TIP3P water molecules. The minimum distance between any solute atom and the edge of the box was 10 Å,[75] resulting in a rectangular box with dimensions of $56.1 \times 50.5 \times 44.9$ Å^3. The solvated system was then subjected to energy minimization, resulting in a RMSD of ~ 1 Å at 0 ps. The MD simulation began by heating up the system from 30 K to 300 K for 10 ps with a temperature-coupling constant of $\tau_T = 0.5$ ps^{-1},[76] and was followed by a MD simulation at 300 K with a temperature coupling parameter of $\tau_T = 0.2$ ps^{-1}. All hydrogen-associated bonds were constrained at their bond lengths with the SHAKE[77] flag on in simulation. A timestep of 2 fs was employed in the MD simulation. The MD trajectory at 300 K after the first 100-ps equilibration was saved every 0.075 ps to calculate ensemble averages of the physical quantities described earlier in the Theory subsection. All the calculations were carried out using the AMBER4.1 package[75] and the Cornell et al. force field was employed to describe the interactions in the system.[78]

In a number of protein simulations,[79–81] the RMSD of these proteins increased to ~ 3.5 Å after ~ 100-ps simulation when a standard 8-Å cutoff method was used to account for long-range, nonbonded interactions.[79–81] The use of a newly developed, more accurate treatment for long-range electrostatic interactions in solution, the PME method,[70] stabilizes the structure of biomolecules at 1.5–2.0 Å.[79–89] Similar to these results, the RMSD of this small basic protein (CTX II) at 300 K, using the 12-Å cutoff of the present study, increased up to ~ 4.0 Å after 100-ps equilibration, as shown in Figure 2. The use of the PME method stabilizes the structure of CTX II in solution at the RMSD of ~ 2.5 Å after 100-ps equilibration (Fig. 2). The rather large RMSD of ~ 2.5 Å in the present simulation is examined in the next section. To remove the overall motion of the entire protein molecule, the coordinates of atoms in each frame of the saved MD trajectories were recalculated such that the RMSD of backbone atoms was minimized with reference to the first frame of the saved trajectory at 300 K. The 400-ps trajectory after 100-ps equilibration at 300 K was used to calculate reorientation order parameters, correlation functions, and B-factors of atomic fluctuation described earlier for CTX II in solution.

The H-bonds in MD simulation described were determined using the following criterion: The distance between hydrogen donor and acceptor is smaller than 3.3 Å and the angle of N—H—O is larger than 130*, and also 50% of the total frames of the saved trajectory satisfies these conditions. The hydrogen bonds are represented by Res1–Res2, where the former residue represents the hydrogen donor, —N—H, and the latter is the acceptor, —C=O. The hydrogen bonds of sidechains are denoted by adding heavy atoms of donors or acceptors of sidechains in the notation of Res1–Res2; for instance, Lys5:N$^\zeta$—Arg36. H-bond denotes hydrogen bond.

Results and Discussion

STRUCTURAL ANALYSIS

The calculated root-mean-square-deviation (RMSD) of CTX II in solution using the PME method is shown in Figure 2 (solid line). After 100-ps equilibration, as described in the method section, the RMSD of CTX II remains at around 2.5 Å. The large derivation in the structure of CTX II in MD simulation occurs at loops, particularly at

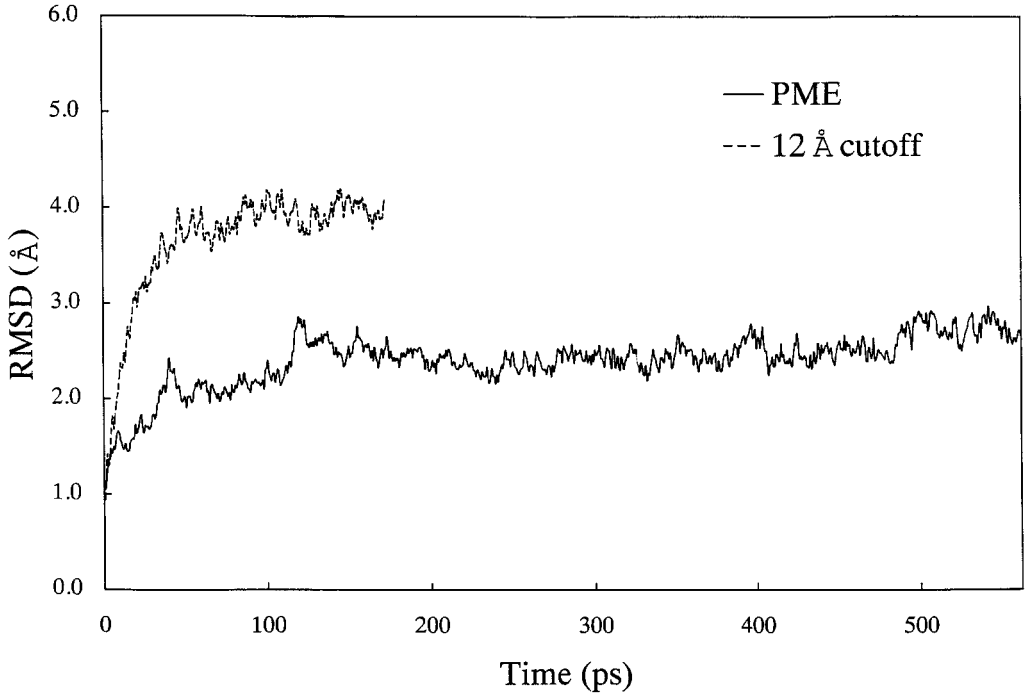

FIGURE 2. Root-mean-square deviation of CTX II along the MD trajectories. Solid line: use of the PME method (see text); dashed line: 12-Å cutoff method.

loop1, where the β1−loop1−β2 segment of the equilibrated MD structure moves further away from the β4-strand, as shown in Figure 3. Similar large separations between β1- and β4-strands are seen in the structures of CTX III[11] and CTX V.[13] Because both sidechains of charged residues, Arg36 of β4-strand and Lys23 of β3 strand, which neighbor each other in space, point toward the backside of protein, the repulsion between these two positively charged sidechains moves the sidechain of Arg36 toward the β1-strand. The movement may result in further separation of the β1−loop1−β2 segment from the β4-strand. Besides this repulsion, the attraction between Arg36 and Asn4 sidechains also drives the Arg36 sidechain toward the β1-strand and forms two H-bonds, Arg36:N^{η}—Asn4:O^{δ} and Lys5:N^{η}—Arg36, between the β1- and β4-strands. The formation of these two new H-bonds drags the β-1 strand closer to the β4-strand, and may thus loosen the interactions between the β-strand and β2-strands. In the loop1 segment, two H-bonds, Leu6—Leu9 and Phe10—Val7, take place in MD simulation. Nevertheless, despite these differences between the NMR and the MD structures, β1- and β2-strands remain at a reasonably close distance. The weakened interaction between β1- and β2-strands results in a structural distortion in MD simulation. These arrangements of H-bonds at the β1-loop1−β2 segment in MD simulation result in a RMSD of $\sim$ 2.5 Å for the equilibrated MD structure from the NMR structure, in which the numbers of NOE restraints for loop1−3 and β1−5-strand segments are 51, 71, 101, and 42, 45, 130, 104, 91, respectively.[16] The low numbers for the loop1, β1-, and β2-strand segments, compared with other loop and β-strand segments, indicate a more flexible and multiconformational structure at these segments. The differences in the structure may arise due to the different force fields used in the present computation and the earlier calculation in determining the NMR structure.[16] Several differences in H-bonding between the equilibrated MD structure and the NMR structure[16] at other places were also observed. The H-bond of Lys18—Ala16 disappears and the H-bond of Lys18—Pro15 is formed. The seven new H-bonds present in MD simulation (Val34—Met24, Met26—Val32, Val27—Leu48, Asn19—Asp40:O^{δ}, Asn45:$N^{\delta 2}$—Tyr51, Tyr51—Asn45:$O^{\delta 1}$, and Ser46—Asn45:$O^{\delta 1}$) strengthen the interactions between β3−5-strands and loop3

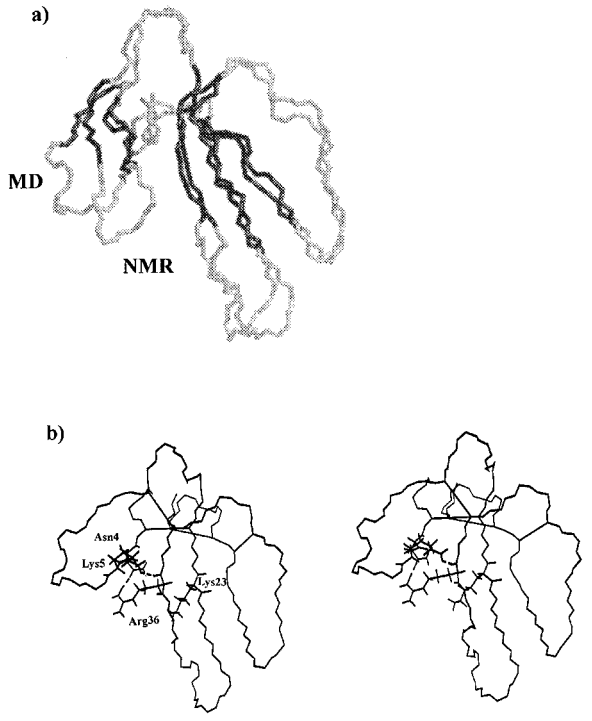

FIGURE 3. (a) Backbone of NMR and MD-equilibrated structures of CTX II. The β-strand and loop segments are shown in black and gray, respectively. (b) Stereoview of MD equilibrated structure with the sidechains displayed as discussed in the text (see text for detailed description).

strands. The equilibrated MD structure at these segments remains close to the NMR structure at a RMSD of $\sim$ 1 Å.

REORIENTATION ORDER PARAMETER

The calculated order parameters of C_α—H bonds are listed in Table I and plotted in Figure 4. The calculated order parameters of C_α—H bonds are generally in good accord with the experimental results. The calculated average order parameters for the secondary structure elements, which agree well with the experimental results, are listed in Table II. With regard to errors in the calculated S^2, as shown by the error bars for the computed S^2 values in the middle plot of Figure 4, a lower S^2 value represents a larger rotational fluctuation of C_α—H bonds accompanying larger errors in the calculated S^2 values obtained from the MD simulation. For many residues of CTX II, the calculated S^2 values are higher than the experimental results by 0.01−0.05, on average, due to the quantum zero point effect,[57,65] which is not included in the present calculation using classical MD simulation, as shown in the bottom plot of Figure 4 for the differences between the computed and experimental S^2 values. The order parameters of residues in β-strands are higher than the residues in loops by $\sim$ 0.05, as found experimentally,[69] except in the case of the β2-strand, in which the calculation gives a lowest S^2 of 0.53 for Lys12. Nonetheless, the highest calculated C_α—H average S^2 value of 0.94 for the β3-strand segment is due to the constraints in four disulfide bonds and many H-bonds on this segment. The S^2 values of residues at loop2, 3 segments show roughly upward curves with higher S^2 values at the end residues of the loop segments, due to neighboring β-strands—except for Ser28, Asn29, and Asn45, which are located in the middle of the loops and have higher S^2 values relative to their neighboring residues. The rather uniform S^2 values of residues in loop1 may be due to the existence of H-bonds of Phe10−Leu7 and Leu9−Leu6 in the equilibrated MD structure, as discussed previously in the Structure Analysis subsection.

In a recent investigation of experimental and computed order parameters, Palmer, Lim, and coworkers developed an excellent new methodology to analyze the accuracy and precision of order parameters obtained from NMR experiments and MD simulations.[90] From several independent sets of NMR relaxation experiments and MD simulations, the accuracy of the order parameters obtained from MD simulations was found to be comparable with experimental results for motions on the rapid timescale of < 100 ps.[90] The computed results of these fast motions have been determined more precisely in MD simulations.[90] Besides, in MD simulations, it was found that the structural distorsion and rare motions are the two most severe artifacts and have a serious influence on the accuracy and precision, respectively, of the computed order parameters.[90] Based on these findings, the order parameters of the ten unobserved residues in the experimental results of CTX II are discussed as follows. Due to structural distortion in the β1−loop1−β2 segment described in the previous subsection, the computed S^2 values of Phe10, Lys12, and Cys14—where the S^2 values of the first two are marked with question marks in Table I because their S^2 values do not meet their correlation functions of internal motion in eq. (5) at a long time duration (see Method section)—may not be accurate. The S^2 values of Gly17, Asn29,

TABLE I.
Order Parameters and Correlation Times of C_α—H Bonds of CTX II.

Residue	2° structure	S^2_{NMR}	S^2_{MD}	τ_{NMR}	τ_{MD}
Leu1		0.72(0.07)	0.73?(0.09)		22.9(12.1)
Lys2	β1	0.86(0.03)	0.87?(0.06)	26.5(15.8)	18.9(8.6)
Cys3	β1	0.80(0.05)	0.91(0.04)	36.8(14.9)	
Asn4	β1	0.89(0.04)	0.83?(0.07)		
Lys5	loop1	0.74(0.07)	0.90(0.05)		13.4(9.7)
Leu6	loop1	0.79(0.04)	0.81(0.07)		28.1(12.2)
Val7	loop1	0.73(0.09)	0.83(0.06)	26.1(15.5)	21.5(10.8)
Pro8	loop1	0.81(0.04)	0.77(0.08)		31.2(7.4)
Leu9	loop1	0.83(0.05)	0.81(0.08)	17.5(15.2)	31.8(11.8)
Phe10	loop1		0.75?(0.09)		29.8(12.4)
Tyr11	β2	0.70(0.04)	0.74?(0.10)	8.3(6.2)	25.1(11.9)
Lys12	β2		0.53?(0.14)		33.8(12.6)
Thr13	β2	0.79(0.05)	0.83?(0.06)	13.1(12.7)	
Cys14			0.81(0.08)		22.9(15.2)
Pro15		0.73(0.04)	0.79(0.07)	6.0(4.8)	
Ala16		0.78(0.04)	0.80(0.06)		
Gly17			0.86(0.05)		
Lys18		0.76(0.05)	0.91(0.04)	14.8(11.1)	
Asn19		0.81(0.08)	0.89(0.04)		
Leu20	β3	0.83(0.04)	0.94(0.03)	28.4(18.7)	
Cys21	β3	0.85(0.05)	0.95(0.02)		
Tyr22	β3	0.88(0.07)	0.95(0.02)		6.7(3.4)
Lys23	β3		0.93(0.03)		9.3(4.4)
Met24	β3	0.82(0.06)	0.94(0.03)		5.0(4.9)
Phe25	β3	0.85(0.06)	0.94(0.03)		8.6(5.9)
Met26	loop2	0.70(0.05)	0.91(0.04)	67.3(12.5)	19.9(6.8)
Val27	loop2	0.79(0.04)	0.78(0.08)	9.7(4.6)	
Ser28	loop2	0.80(0.03)	0.81(0.07)		22.8(11.3)
Asn29	loop2		0.85(0.05)		
Leu30	loop2	0.74(0.03)	0.72(0.09)	65.4(9.3)	
Thr31	loop2		0.84(0.06)		18.9(7.4)
Val32	loop2	0.75(0.11)	0.87(0.05)		29.8(7.7)
Pro33	loop2	0.75(0.05)	0.89(0.04)	16.2(9.4)	14.3(6.4)
Val34	β4	0.90(0.04)	0.92(0.03)		14.3(4.6)
Lys35	β4	0.91(0.05)	0.93(0.03)		
Arg36	β4	0.88(0.04)	0.93(0.03)		6.4(5.3)
Gly37	β4		0.86(0.04)		
Cys38	β4	0.89(0.03)	0.88(0.05)		22.2(8.1)
Ile39	β4	0.86(0.07)	0.95(0.03)	43.2(31.3)	
Asp40	loop3	0.75(0.06)	0.91(0.04)	18.2(7.8)	
Val41	loop3	0.85(0.03)	0.88(0.05)		
Cys42	loop3	0.84(0.05)	0.87(0.06)	15.8(13.6)	33.1(7.7)
Pro43	loop3	0.77(0.04)	0.63?(0.12)		45.5(8.9)
Lys44	loop3	0.80(0.05)	0.66?(0.11)	20.6(11.5)	
Asn45	loop3		0.88(0.05)		
Ser46	loop3	0.77(0.04)	0.82(0.07)		13.4(11.4)
Ala47	loop3	0.76(0.04)	0.81?(0.06)	15.9(9.4)	
Leu48	loop3	0.76(0.08)	0.83(0.06)	23.8(16.3)	12.3(10.9)
Val49	loop3	0.83(0.04)	0.91(0.04)		19.1(8.2)
Lys50	β5		0.88(0.06)		14.9(11.1)
Tyr51	β5	0.65(0.09)	0.94(0.02)		
Val52	β5	0.85(0.03)	0.91(0.04)	15.0(7.6)	20.5(5.6)

TABLE I.
Continued

Residue	2° structure	S^2_{NMR}	S^2_{MD}	τ_{NMR}	τ_{MD}
Cys53	β5	0.81(0.08)	0.90(0.04)		
Cys54	β5	0.87(0.07)	0.89?(0.05)		
Asn55		0.83(0.04)	0.88?(0.05)		
Thr56		0.76(0.07)	0.86(0.05)		
Asp57		0.79(0.04)	0.76?(0.09)	23.3(7.8)	30.8(9.8)
Arg58		0.72(0.12)	0.82?(0.07)		32.2(10.7)
Cys59		0.65(0.13)	0.82?(0.08)		
Asn60		0.83(0.05)	0.54?(0.14)	12.8(12.4)	51.9(11.1)

β denotes β-strands. Numbers in parentheses are errors of the corresponding calculated quantities. Question marks are placed next to S^2 values of residues whose calculated S^2 do not meet the values of their correlation functions at long time scales (see text).

Thr31, and Asn45, which are located in the tip or loop segments, and are not involved in any H-bonding, are less certain because the timescale of their backbone motion may be greater than the nanosecond range. The most certain are the high S^2 values of Lys23, Gly37, and Lys50, which are located in β3-, β4, and β5-strands, respectively, and are all involved in the H-bondings of the β3–β4 − B1β5 anti-β-sheet of CTX II.

In addition to C_α—H bonds, the order parameters of the N—H bonds on the backbone of CTX II were also calculated, as shown in Figure 5. The S^2 values of N—H bonds are less uniform and lower than those of C_α—H bonds for most residues, due to the better ability of hydrogen exchange with water for the hydrogens of N—H bonds than the hydrogens of C_α—H bonds, as found with other proteins in solution.[57,65] Similar to the high S^2 values of C_α—H bonds in β-strands relative to other secondary segments, except in the case of the β2-strand described earlier, the S^2 values of N—H bonds in β-strands are higher than other sec-

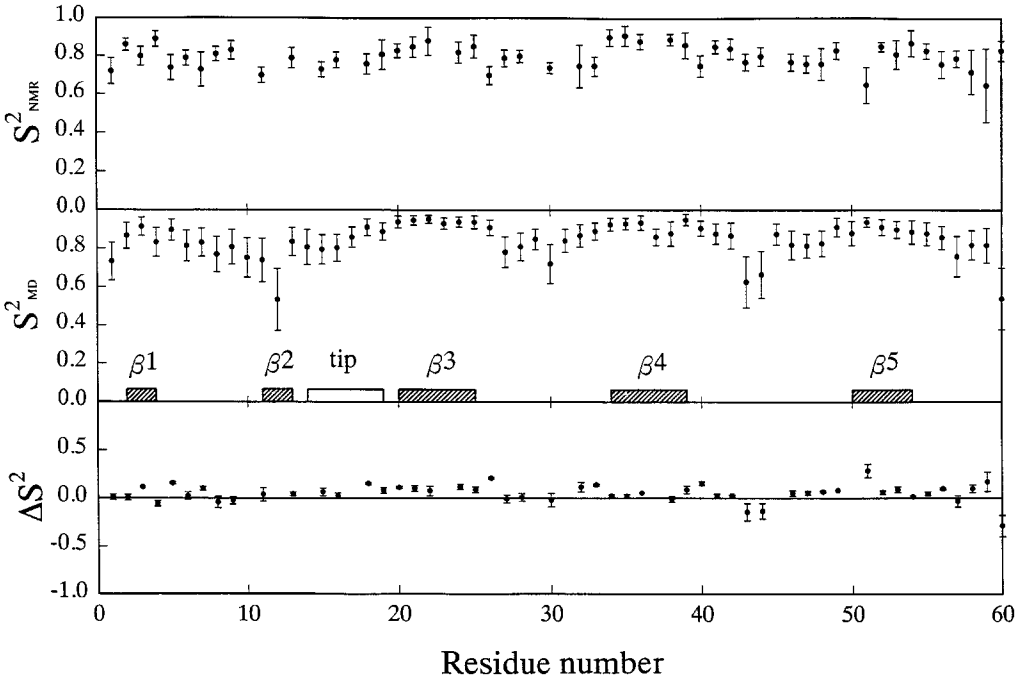

FIGURE 4. Order parameters of C_α—H bonds of CTX II. Upper plot: experimental results; middle plot: computed results; lower plot: differences between computed and experimental results.

TABLE II.
Averaged Order Parameters of C_α—H Bonds of CTX II.

2^0 structure	Residue number	S^2_{NMR}	S^2_{MD}	S^2_{NMR} avg.	S^2_{MD} avg.
N-terminal	1	0.72	0.73	0.72	0.73
β1-strand	2–4	0.85	0.87		
β2-strand	11–13	0.75	0.70		
β3-strand	20–25	0.85	0.94	0.84[a]	0.86[a]
β4-strand	34–39	0.89	0.91		
β5-strand	50–54	0.80	0.90		
Tip	14–19	0.77	0.84	0.77	0.84
Loop1	5–10	0.78	0.81		
Loop2	26–33	0.76	0.83	0.78[b]	0.82[b]
Loop3	40–49	0.79	0.82		
C-terminal	55–60	0.76	0.78	0.76	0.78

[a] Average S^2 value for residues in all β-strands.
[b] Average S^2 value for residues in all loop segments.

ondary segments as well, despite the exception of a few residues. The details of these calculated order parameters, on the basis of secondary structures and interactions between residues, are discussed further in what follows.

β-strands. The calculated S^2 values of C_α—H bonds for all residues in β-strands are higher than experimental results, except in the case of Asn4 and Cys38, as shown in Figure 2. Both experiment and computation give the lowest average S^2 values at the β2-strand among all β-strand segments (Table II). The higher average calculated S^2 values of β3- and β5-strands compared with the experimental results (by ~ 0.1) is due to the additional H-bonds of Asn19—Asp40, Asn45:$N^{\delta 2}$—Tyr51, Tyr51—Asn45:$O^{\delta 1}$, and Val27—Leu48, which were observed in the MD trajectory but not in the NMR structure. Besides, the two other H-bonds of Val34

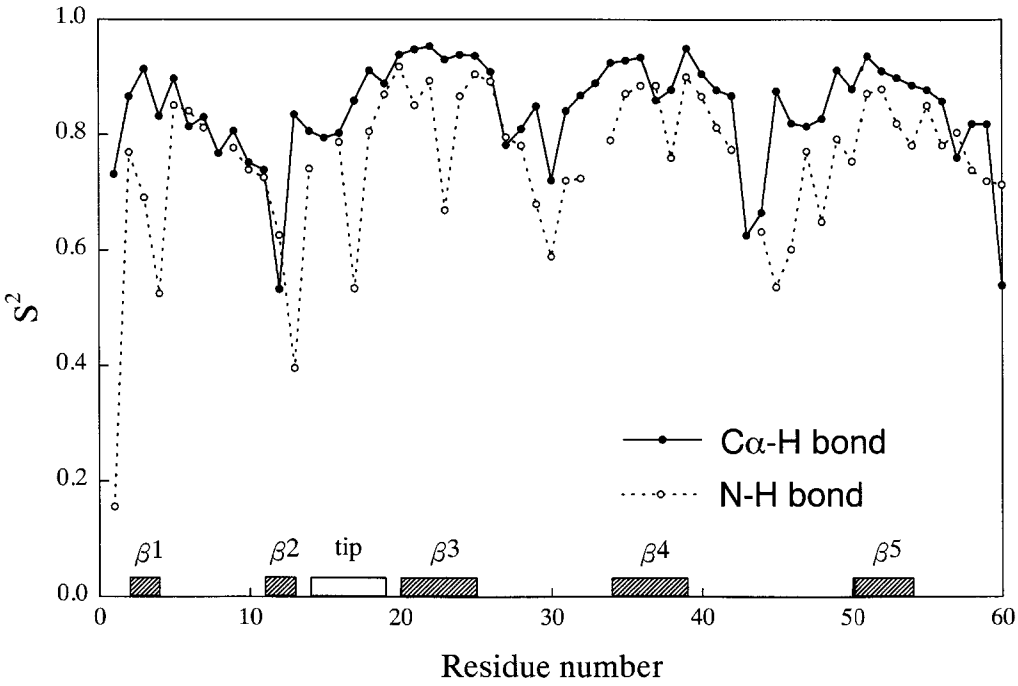

FIGURE 5. Computed order parameters of C_α—H and N—H bonds of CTX II.

—Met24 and Met26—Val32, which occurred only in MD simulation, may also strengthen the interactions on the β3-strand and reduce its mobility. However, the effect of these added interactions on the mobility of the β4-strand is not significant where experiment and computation give close S^2 values of 0.89 and 0.91, respectively. The average calculated S^2 values of the β1 strands are also in agreement with the experimental results; however, the individual calculated S^2 value of each residue alternates in an opposite way to the experimental results in this segment. The discrepancy may arise from the distortion of the structure at the β1−loop1−β2 segment in MD simulation as described earlier.

Among all β-strands, except for residues of the β1 and β2 strands (which show greater structure fluctuations due to weak interactions between them as well as Gly37 and Cys38 of β4-strand with S^2 values lower than neighboring residues) computation gives relatively high S^2 values of C_α—H bonds for all residues in β-strands. The low S^2 value of Cys38 is because it is the only residue in which the H-bond is not involved in the β3−5 strands, which indicates that the disulfide bond of Cys38—Cys14 does not have a significant effect in restraining the rotational motion of the C_α—H bond of Cys38. The relatively low B-factors of cysteines (see Figure 8 of B-factor subsection below) all show a small backbone fluctuation in translational degrees of freedom. The structural restraint due to the presence of disulfide bonds through sidechains of cysteines gives a significant effect in structural fluctuation in translational degree of freedom. In the β2-strand, the computation gives the lowest S^2 value for Lys12 due to the weak interactions between β1- and β2-strands described earlier. Calculation of ϕ and ψ angles for Lys12 indicates two significantly different local conformations in MD trajectory, as shown in Figure 6.

Similar to the high S^2 values of C_α—H bonds for residues in β-strands, the calculated S^2 values of N—H bonds for residues in β-strands are higher than the other secondary segments as well, except in the cases of Lys2, Lys23, and Cys38 of β1-, β2-, and β4-strands, respectively. In the β1-strand, the S^2 values of the C_α—H bonds are rather uniform as compared with the other β-strands. The decreasing S^2 values of N—H bonds from Lys2 to Asn4 show a small local N—H bond rotational fluctuation at Lys2 and a large fluctuation of the N—H bond at Asn4. In the β2-strand, low S^2 values of both C_α—H and N—H bonds for Lys12, and very low S^2 value of the N—H bond and

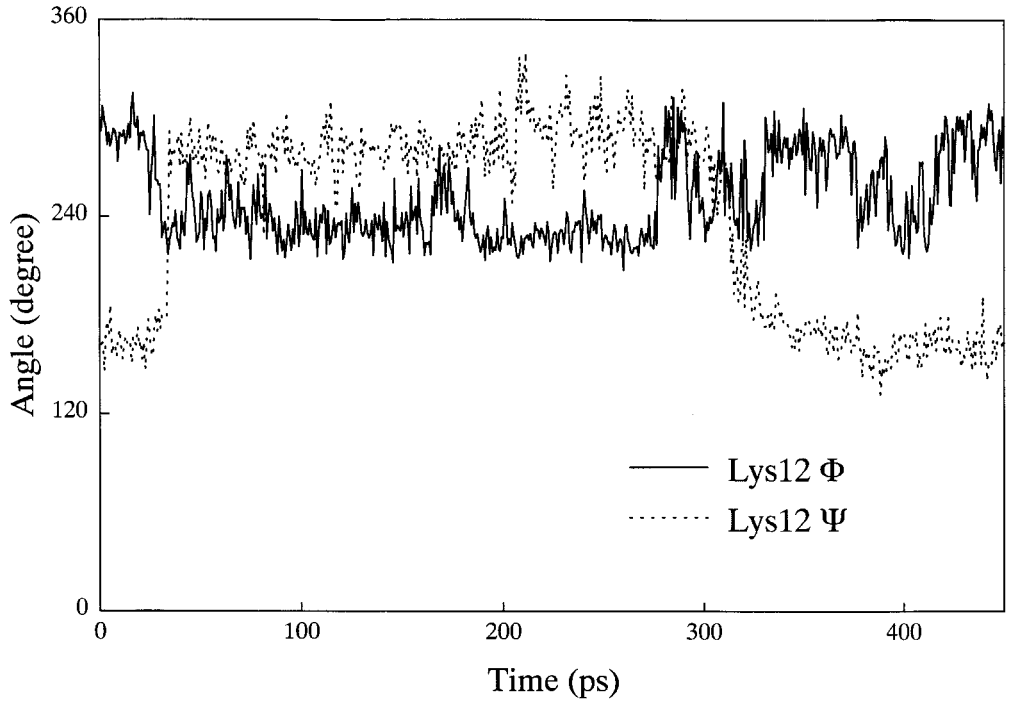

FIGURE 6. The ϕ and ψ angles of Lys12 along the MD trajectory.

high S^2 value of the C_α—H bond for Thr13, show that larger backbone fluctuation occurs between Lys12 and Thr13 than on the spot between Tyr11 and Lys12. In the β4-strand, computation indicates low S^2 values of N—H bond for Val34 located at one end of the β4-strand, and at the other end Cys38 has a low S^2 value but Ilu39 has a high value due to the H-bond of Ile39—Leu20. In the β5-strand, which neighbors the flexible loop3 segment, computation gives low S^2 values for Lys50 and Cys54, which are located at two ends of the β5 strand. Besides, the other low S^2 values of N—H bonds in β-strands are located at the end of β-strands where large fluctuation occurs due to the neighboring flexible loops. In comparison to the S^2 values of C_α—H and N—H bonds for residues of β-strands shown in Figure 5, high S^2 values of C_α—H bonds do not always accompany high S^2 values of N—H bonds, indicating the presence of very local structural fluctuation on the backbone,

Loops. The calculated average S^2 values of C_α—H bonds for the loop segments listed in Table II are lower than β-strands, with a difference of 0.04, which is in good accord with the difference of 0.06 between the average S^2 value of loop and β-strand segments obtained from an NMR experiment.[69] The much higher calculated S^2 values of Met26 and Asp40 than the experimental results, by 0.21 and 0.16, respectively, is due to the presence of H-bonds of Met26—Val32 and Asn19—Asp40:O^{δ}, which do not exist in the NMR structure, but are present in the MD trajectory. The high calculated S^2 values of Val32 and Pro33 are also attributed to the additional H-bonds of Met26—Val32 and Val34—Met24 in the MD trajectory. In the loop1 segment, the experimental S^2 values of residues start low at Lys5, and alternate in segments from Leu6 to Phe10. On the other hand, the calculated S^2 values of residues alternate in this segment in contrast to the high value at Lys5 due to H-bonds of Leu6—Leu9 and Phe10—Val17. The high S^2 values of C_α—H bonds in the hydrogen acceptors Val17 and Leu9 compared with hydrogen donors Leu6 and Phe10 suggest that the H-bonds add more restraint to the rotational motion of C_α—H bonds for hydrogen acceptor residues than hydrogen donor residues. For residues in the loop2 segment from Met26 to Pro33, and loop3 segment from Asn40 to Val49, the S^2 values of these two loops form roughly upward curves, with the exception of higher S^2 values at Ser28 and Asn29 of loop2 and Asn45 of loop3 relative to their neighbor residues as shown in Figure 4. The high S^2 value of Asn45 is attributed to the two H-bonds between the sidechain of Asn45, and —N—H and —C=O of Tyr51.

In Figure 5, showing the calculated order parameters for both C_α—H and N—H bonds, the high S^2 values of N—H bonds for Lys5, Leu6, Val7, Leu9, and Phe10 in the loop1 segment may be due to the constraints arising from the H-bonds between Leu6—Leu9 and Phe10—Val7 on the backbone and the two H-bonds between the sidechains of Lys5 and Arg36. In the loop 2 segment, unlike the higher S^2 values of the C_α—H bonds for Ser28 and Asn29 relative to their neighboring residues, the S^2 values of N—H bonds in this segment show an upward curve and reach the lowest point at Leu30, located at the center of the loop2 segment. The S^2 values of N—H bonds in loop3 show an upward curve as well except in case of the high S^2 value of 0.87 for Ala47 relative to its neighbors. This may be due to the presence of the H-bonds of Ser46—Asn45:$O^{\delta 1}$ and Val27—Leu48 in MD simulation, which add to the constraint in backbone flexibility at Ala47. The high S^2 value of the C_α—H bond but low S^2 value of the N—H bond for Asn45 suggest that the bifurcated H-bond between the sidechain of Asn45 and —C=O of Tyr51 and —N—H of Ser46 restrains the rotational flexibility of the C_α—H bond of Asn45 more than the N—H bond.

Tip, N-, and C-termini. The calculated S^2 values of C_α—H residues in the tip segment and N- and C-termini (Fig. 4) are all higher than the experimental values, except for Asp57 and Asn60, which are located in the center of a small loop segment from Asn55 to Cys59 and the very end of the C-terminal, respectively. The higher calculated S^2 value of Cys59 compared with the experimental result is due to the H-bond of Asn60—Thr59 present in the MD trajectory but not in the NMR structure. The higher calculated S^2 value of Lys18 in the tip segment compared with experimental results (by 0.15) indicates an overestimated constraint at the head region of CTX II in the MD simulation. Similar to S^2 values of C_α—H bonds for residues in loop segments, which show roughly upward curves in Figure 4, the S^2 values of C_α—H bonds at the two ends of the tip segment are higher than those in the center. While the β-sheet structure of the β1−loop1−β2 segment was distorted in the MD simulation, the loose interactions between the β1- and β2-strands resulted in low S^2 values of the C_α—H bond of Ly12 and N—H bonds of Lys12 and Thr13. The high S^2 value of

Lys18 and Asn19 is due to the respective H-bonds of Lys18—Pro15 and Asn19—Asp40:O^{δ}, and also because of the less flexible neighboring β3-strand. In the C-terminal segment, the Cys54—Cys59 disulfide bond and the Cys59—Thr56 H-bond form a small loop in this segment, for which the computation gives a low S^2 value for the C_{α}—H bond of Asp57 located in the center of this small loop and high S^2 values for Cys54, Thr56, and Cys59 found at the end of the segment. Furthermore, the low S^2 values for the C_{α}—H bonds of both Leu1 and Asn60 show a large backbone fluctuation at the termini.

In Figure 5, the S^2 values of N—H bonds for Asn55 and Asp57 are higher than their neighbors, Cys54 and Thr56, which possess H-bonds during the MD trajectory, indicating small local rotational fluctuation in the N—H bond motion at these two residues. At the N-terminal, the computation gives a low S^2 value of 0.15, showing a free rotational motion of N—H bonds at the very end of the N-terminal. At the C-terminal, Asn60 has a lower S^2 value for the C_{α}—H bond than for the N—H bond: (1) because it is closer to the extreme end of the C-terminal than the N—H bond; and (2) because of the existence of the H-bond of Asn60—Thr56, which adds constraint to the flexibility of the N—H bond of Asn60 in MD simulation.

CORRELATION FUNCTION AND CORRELATION TIME

The reorientation autocorrelation function of the C_{α}—H bond for each residue was calculated in eq. (1). Following the ref. 57, the correlation functions of the residues are categorized into four classes, to which the correlation functions of the four representative residues (Leu20, Cys42, Arg58, and Lys12) belong, as shown in Figure 7. These are: class I—the correlation function decays within 20 ps to a well-defined plateau value; class II—the corrected decay time is longer than 20 ps; class III—the function decays to a plateau value in a short time, then decays further, but no plateau is reached; and class IV—no well-defined plateau value is reached within the 180-ps correlation time. Among all residues, 26 residues belong to the class I category, which are of high S^2 values and short correlation times. 16 residues of them are located in the β-strands and the other 10 residues are located in other segments. In the class II category which contains 18 residues, and has moderately high S^2 values, only Lys3 and Gly37 are located in the β-strands, whereas the other residues in this class are located in other segments. The remaining residues in the protein, which are of relatively low S^2 values and located mostly in loops, tip, and N- and C-termini, belong to either classes III or IV, and their S^2 values are marked with question marks because the values of these correlation functions at long time do not meet their S^2 values. Interestingly, the correlation functions of all prolines belong the the classes III and IV. Cyclization of sidechain onto the backbone results in an uncertain S^2 values for prolines in the present subnanosecond MD simulation. In the cases of Met26 and Asn60 residues, the calculated correlation times differ significantly from experimental correlation times by about threefold; computation also shows large differences between calculated and experimental S^2 values by more than 0.2.

B-FACTOR

The calculated B-factors are plotted together with CTX V, as shown in Figure 8, which is the only available crystal data of CTX from the Taiwan cobra venom. Because CTX II and CTX V are of 65% homology and they contain 60 and 62 residues, respectively, the alignment based on their homology results in broken data in the MD simulation at Res4 and Res31. To remove the effect due to lattice disorder (crystal heterogeneity),[91] and the experimental B-factor values are downshifted by 0.51 Å^2 following Refs. 57 and 91. The calculated B-factors are in good accord with the crystal data, where the loop segments show greater fluctuations than β-strands, except for the β2 strand, and they are consistent with the atomic fluctuation of backbone found in a previous MD simulation, in which loop1 and tip segments also showed high fluctuations (as shown in Fig. 7 of Ref. 16). The large B-factors are in contrast to low-order parameters and vice versa as shown in Figures 5 and 8. In general, large transational fluctuation of residues with large B-factor values results in a large rotational fluctuation of low-order parameters of C_{α}—H or N—H bonds as well. Among all secondary structures, except for loop1, loop3, N- and C-termini, and β2-strand segments, the calculated B-factors of residues of CTX II in solution are smaller than the crystal data of CTX V.[20] The reason for the higher calculated S^2 values than experimental S^2 values is the same as described earlier; the underestimation of B-factors is likely due to the excluded quantum zero point energy in the present classical MD simulation, which has also been found in other protein simulations.[57, 65]

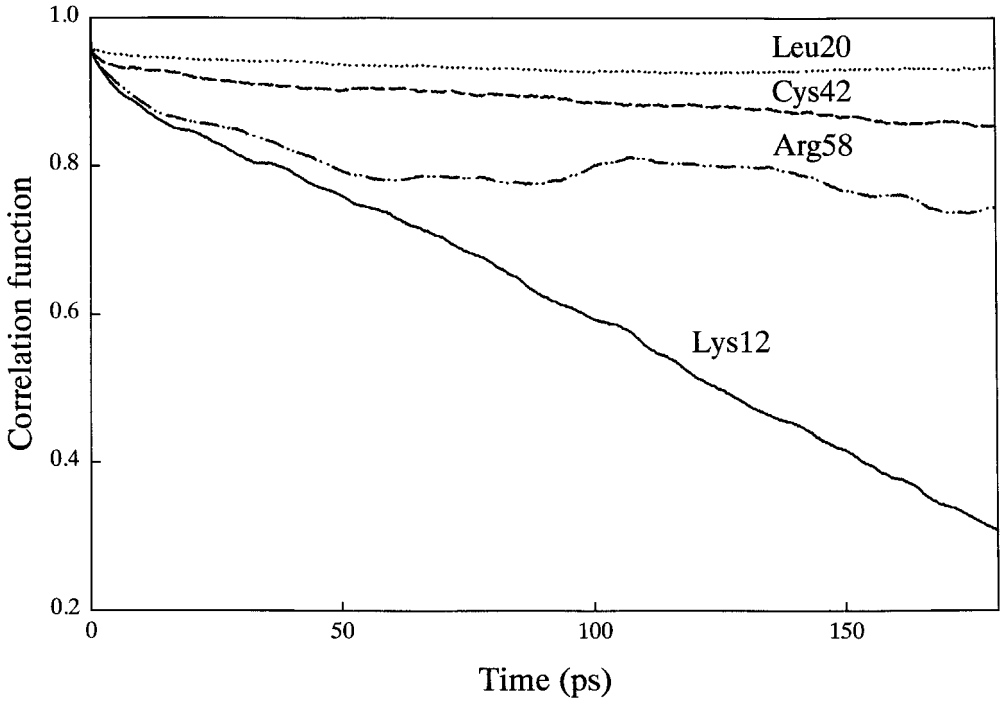

FIGURE 7. Typical C_α—H bond reorientation autocorrelation functions of CTX II (see Results).

In the loop2 segment, which is constrained by many H-bonds between β3-m β4-, and β5-strands, the calculated B-factors are lower than those in loop1 and loop3, which agrees well with experimental results. The high flexibility at the β2-strand is due to the loose interactions in MD simulation described earlier. In the cases of loop1, loop3, and N- and C-termini of large B-factors, because the crystal packing of CTX V monomers in the crystal state is assisted by hydrophobic interactions at the sites of contact of the three loops between the monomers,[20] solvation of CTX releases interactions due to the hydrophobic effect at the loop region between the monomers in the crystal, which results in larger B-factors in solution at loop1, loop3, and terminal segments. Further analysis of calculated B-factors in a basis of secondary structure elements is examined in what follows.

β-Strands. The calculated low B-factors of residues in β-strands of CTX II from MD simulation are in good accord with crystal data of CTX V, as shown in Figure 8, except for significant differences at the β2-strand, Cys38 and Ile39 of the β4-strand, and Tyr51 and Val52 of the β5-strand in CTX II whose computed B-factors are greater than the experimental values. The computed B-factor values of residues in β-strands are in contrast to the calculated S^2 values of C_α—H bonds in Figure 5, showing a large fluctuation of heavy atoms on the backbone in both translational motion and rotational motion of C_α—H bonds, except in the case of Gly37 and Cys38, for which the lower B-factors and higher S^2 values of C_α—H bonds relative to their neighboring residues reflect a high C_α—H bond rotational flexibility but low transitional flexibility of the backbone.

Loops. For B-factors of loop 1–3 segments, the computed B-factors of the residues of loop2 agree well with the experimental results due to the constraint arising from the H-bonds between the β3- and β4-strands, which restrain the flexibility of loop2 and result in lower B-factors for most residues in loop2 than the experimental results. Significant differences at loop1 and loop3 may be due to the solvation of protein in solution from the crystal structure and the disappearance of hydrophobic interactions at loop regions between the CTX monomers in crystal.[20] The computed B-factors of residues in loop segments are in contrast to the computed S^2 values in Figure 5, except for the very high B-factors of Val7 and Pro8, but high S^2 values for the N—H bond of Val7 and for C_α—H bonds of both Val7 and Pro8. The large transational structure fluctuation of Val7 and Pro8 does not result in large rotational flexibility in the N—H

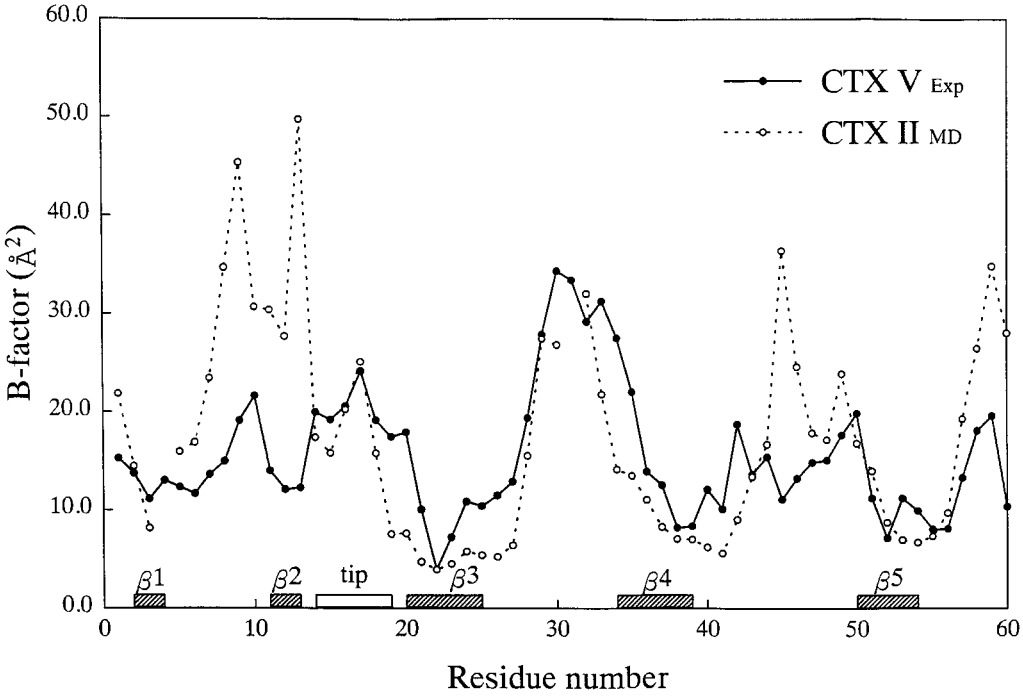

FIGURE 8. B-factors of CTX in solution. Closed circles: available crystallography data of CTX V; open circles: computed B-factors of CTX II in solution.

bond of Val7 and in C_α—H bonds of both Val7 and Pro8. While in the cases of Ser28 and Val29, computation gives nearly equal B-factors and S^2 values of C_α—H bonds but a lower S^2 value of N—H bond for Val29 than for Ser28.

For N-, and C-termini, the calculated S^2 values of C_α—H the computed B-factors of residues bonds and the tip segment are also in agreement with experimental results, except for a significant difference at the C-terminal segment. At these segments, as shown in Figure 5, the computed B-factors are in contrast to the calculated S^2 values of C_α—H and N—H bonds except in the case of the S^2 value for the N—H bond of Gly17. The low B-factor and S^2 value of the N—H bond, but high S^2 value of C_α—H bond for Gly17, indicate that the translational motion of backbone and rotational motion of the C_α—H bond at Gly17 is less flexible while accompanying the large rotational flexibility of the N—H bond.

CORRELATION WITH BIOLOGICAL FUNCTION

Much progress has been made in understanding the actions of CTXs and their biological functions during the past few years.[2, 5, 29–37] Examination of key residues in binding with biomolecules has been the focus of efforts to interpret the variations in biological activity among CTXs. In a series of experiments conducted to investigate the interaction of CTXs with membrane, key residues have been identified and their roles have been fully examined.[2, 23–25] Based on the homology of CTXs and their correlation to biological activities, several types of CTXs were distinguished.[2, 5, 33–36] In addition, significant progress has been made in investigating the binding modes and structure of CTX–substrate complexes.[2, 5, 33–35, 92–94] The detailed structure of the CTX/dATP complex has been resolved in a recent NMR NOESY experiment.[37] In experiments conducted to assess the role of residues in CTXs,[29–32] several reserved Met and Lys residues in CTXs were found to have a crucial role on CTX toxicity.[29–32] From the experimental results of order parameters for C_α—H bonds of CTX II, among these Met and Lys residues, the high backbone mobility at Met24, Met26, Lys5, Lys18, and Lys44 was correlated to the biological functions of CTXs, because high mobility suggests easier adoption of substrates.[69] In the MD simulation, the computed high C_α—H order parameters for the first four of these residues and the underestimated computed S^2 values for Lys44 do not agree with experimental results. We do not know the physical reason for these discrepancies. A possible artifact causing the differences

in S^2 values for the latter three lysines is the presence counterions, which were initially placed at the beginning of the MD trajectory close to the sidechains of these lysines and located ''on the surface'' of this small protein in the present simulation protocol. However, examination of movement of these counterions in the MD trajectory shows that they were solvated by water molecules and moved into bulk of water during a < 100-ps simulation at 300 K, and thus should not significantly influenced the backbone dynamics of these lysines.

In summary, molecular dynamics simulation of CTX II in an explicit water model was carried out to examine backbone mobility in solution, wherein a newly developed, more accurate treatment for long-range electrostatic interactions was employed in simulation. The calculated order parameters of C_α—H bonds and B-factors for backbone fluctuation, overall, agreed well with the experimental results qualitatively and were of aid in the interpretation of experimental data regarding backbone dynamics. The calculated S^2 values of many residues are also in quantitatively good agreement with the experimental results. The difference in the computed average lower S^2 values of residues in loop segments and the average higher S^2 values of residues in β-strands is in good accord with experimental results. However, the physical basis of the disagreement between the computed and the NMR results for those residues, whose calculated S^2 values differ significantly from NMR-derived data, was not clear from the present study. The discrepancy between the present MD results and experimental results may arise from structural distortion and the subnanosecond timescale sampling in our MD simulation. Examination of accuracy and precision of the calculated order parameters in the present computation following the newly developed methodology[90] should be the subject of future study.

Acknowledgments

The authors thank Prof. C. Yu and Prof. C. Lim for helpful discussions, and the NMR work prior to publication provided by Prof. Yu. Y.C.S. thanks Prof. Peter A. Kollman for encouragement during his stay at UCSF. We are grateful for helpful discussion with Prof. W. G. Wu. Many thanks are due to Prof. W. C. Huang, Drs. C. D. Hsiao, C. S. Lee, and C. M. Chiang for useful discussions. Ms. Shih is thanked for her help in preparing the manuscript. The NCHC is acknowledged for providing CPU time.

References

1. Yu, C.; Bhaskaran, R.; Yang, C. C. J Toxicol Toxin Rev 1994, 13, 91–315.
2. Wu, W. J Toxicol Toxin Rev 1997, 16, 115–134 (and references therein).
3. Kumar, T. K. S.; Jayaraman, G.; Lee, C. S.; Arunkumar, A. I.; Sivaraman, T.; Samuel, D.; Yu, C. J Biomol Struct Dyn 1997, 15, 431–463.
4. Kumar, T. K. S.; Pandian, S. K.; Srisailam, S.; Yu, C. J Toxicol Toxin Rev. In press.
5. Chien, K. Y.; Huang, W. N.; Jean, J. H.; Wu, W. J Biol Chem 1991, 266, 3252–3259.
6. Louw, A. I.; Visser, L. Biochim Biophys Acta 1978, 512, 163–171.
7. Harvey, A. L.; Hider, R. C.; Khader, F. Biochim Biophys Acta 1983, 728, 215–221.
8. Yang, C. C. Biochim Biophys Acta 1967, 133, 346.
9. Yang, C. C.; Chang, C. C.; Hayashi, K.; Suzuki, T. Toxicon 1969, 7, 43.
10. Yang, C. C.; Yang, H. J.; Huang, J. S. Biochim Biophys Acta 1969, 188, 65.
11. Bhaskaran, R.; Huang, C. C.; Chang, D. K.; Yu, C. J Mol Biol 1994, 235, 1291–1301.
12. Bhaskaran, R.; Yu, C.; Yang, C. C. J Prot Chem 1994, 13, 503–504 (and references therein).
13. Singhal, A. K.; Chien, K. Y.; Wu, W.; Rule, G. S. Biochemistry 1993, 32, 8036–8044.
14. Kumar, T. K. S.; Lee, C. S.; Yu, C. Natural Toxins 1996, 115–129.
15. Yu, C.; Bhaskaran, R.; Chuang, L. C.; Yang, C. C. Biochemistry 1993, 32, 2131–2136.
16. Bhaskaran, R.; Huang, C. C.; Tsai, Y. C.; Jayaraman, G.; Chang, D. K.; Yu, C. J Biol Chem 1994, 38, 23500–23508. After finishing computations in this study, we learned that the new structure of CTX II using high-resolution NMR was published (Jang et al. 1997). Computations using this new structure are currently under way.
17. Jang, J. Y.; Kumar, T. K. S.; Jayaraman, G.; Yang, P. W.; Yu, C. Biochemistry 1997, 36, 14635–14641.
18. Sivaraman, T.; Kumar, T. K. S.; Yang, P. W.; Yu, C. Toxicon 1997, 35, 1367–1371.
19. O'Connell, J. F.; Bougis, P. E.; Wuthrich, K. Eur J Biochem 1993, 213, 891–900.
20. Sun, Y. J.; Wu, W.; Chiang, C. M.; Hsin, A. Y.; Hsiao, C. D. Biochemistry 1997, 36, 2403–2413.
21. Jayaraman, G.; Kumar, T. K. S.; Sivaraman, T.; Lin, W. Y.; Chang, D. K.; Yu, C. Biol Macromol 1996, 18, 303–306.
22. Sivaraman, T.; Kumar, T. K. S.; Yu, C. Biol Macromol 1996, 19, 235–239.
23. Chiang, C. M.; Chang, S. L.; Lin, H. J.; Wu, W. Biochemistry 1996, 35, 9177–9186.
24. Chiang, C. M.; Chien, K. Y.; Lin, H. J.; Lin, J. F.; Yeh, H. C.; Ho, P. I.; Wu, W. Biochemistry 1996, 35, 9167–9176.

25. Wu, C. Y.; Chen, W. C.; Ho, C. L.; Chen, S. T.; Wang, K. T. Biochem Biophys Res Commun 1997, 233, 713–716.
26. Sivaraman, T.; Kumar, T. K. S.; Jayarman, G.; Han, C. C.; Yu, C. Biochem J 1997, 321, 457–464.
27. Sivaraman, T.; Kumar, T. K. S.; Jayaraman, G.; Yu, C. J Prot Chem 1997, 16, 291–297.
28. Sivaraman, T.; Kumar, T. K. S.; Chang, D. K.; Lin, W. Y.; Yu, C. J Biol Chem 1998, 273, 10181–10189.
29. Carlsson, F. H. H.; Louw, A. I. Biochem Biophys Acta 1978, 534, 322–330.
30. Gatineau, E.; Toma, F.; Montenary-Garestier, T.; Takechi, M.; Fromageot, P.; Menez, A. Biochemistry 1987, 26, 8046–8055.
31. Dufton, M. J.; Hider, R. C. The structure and pharmacology of elapid cytotoxins in snake toxins (ed. A. L. Harvey); Pergamon: New York; 1991, pp 259–302.
32. Surewicz, W. K.; Stepanik, T. M.; Szabo, A. G.; Mantsch, H. H. J Biol Chem 1988, 263, 786–790.
33. Vyas, A. A.; Patel, H. V.; Pan, J. J.; Vyas, K. A.; Chiang, C. M.; Sheu, Y. C.; Hwang, J. K.; Wu, W. J Biol Chem 1997, 272, 9661–9670.
34. Patel, H. V.; Vyas, A. A.; Vyas, K. A.; Liu, Y. S.; Chiang, C. M.; Chi, L. M.; Wu, W. J Biol Chem 1997, 272, 1484–1492.
35. Chien, K. Y.; Chaing, C. M.; Hseu, Y. C.; Vyas, A. A.; Rule, G. S.; Wu, W. J Biol Chem 1994, 269, 14473–14483.
36. Sue, S. C.; Rajan, P. K.; Chen, T. S.; Hsieh, C. H.; Wu, W. Biochemistry 1997, 36, 9826–9836.
37. Jayaraman, F.; Kumar, T. K. S.; Yu, C. Annual Meeting of the Chinese Chemical Society; 1997.
38. Mandel, A. M.; Akke, M.; Palmer, A. G. J Mol Biol 1995, 246, 144–163.
39. Clubb, R. T.; Omichinski, J. G.; Sakaguchi, K.; Appella, E.; Gronenborn, A. M.; Clore, G. M. Prot Sci 1995, 4, 855–862.
40. Farrow, N. A.; Muhandiram, R.; Singer, A. U.; Pascal, S. M.; Kay, C. M.; Gish, G.; Shoelsen, S. E.; Pawson, T.; Forman-Kay, J. D.; Kay, L. E. Biochemistry 1994, 33, 5984–6003.
41. Mispelter, J.; Lefevre, C.; Adjadj, E.; Quiniou, E.; Favaudon, V. J Biomolec NMR 1995, 5, 233–244.
42. Borer, P. N.; LaPlante, S. R.; Kumer, A.; Zanatta, N.; Martin, A.; Hakkinen, A.; Levy, G. C. Biochemistry 1994, 33, 2441–2450.
43. Stone, M. J.; Chandrasekhar, K.; Holmgren, A.; Wright, P. E.; Dyson, J. J. Biochemistry 1993, 32, 426–435.
44. Akke, M.; Skelton, N. J.; Kordel, J.; Palmer, A. G.; Chazin, W. J. Biochemistry 1993, 32, 9832–9844.
45. Akke, M.; Bruschweiler, R.; Palmer, A. G. J Am Chem Soc 1993, 115, 9832–9833.
46. Stone, M. J.; Fairbrother, W. J.; Palmer, A. G.; Reizer, J.; Seier, Jr., M. H.; Wright, P. E. Biochemistry 1992, 31, 4394–4406.
47. Palmer, A. G.; Rance, M.; Wright, P. E. J Am Chem Soc 1991, 113, 4371–4380.
48. Clore, G. M.; Driscoll, P. C.; Wingfield, P. T.; Gronenborn, A. M. Biochemistry 1990, 29, 7387–7401.
49. Kay, L. E.; Torchia, D. A.; Bax, A. Biochemistry 1989, 28, 8972–8979.
50. Dellow, M. J.; Wand, A. J. J Am Chem Soc 1989, 111, 4571–4578.
51. Nirmala, N. R.; Wanger, G. J Am Chem Soc 1998, 110, 7557–7558.
52. Lipari, G.; Szabo, A. J Am Chem Soc 1982, 104, 4546–4559.
53. Lipari, G.; Szabo, A. J Am Chem Soc 1982, 104, 4559–4570.
54. Wittebort, R. J.; Szabo, A. J Chem Phys 1978, 69, 1722–1736.
55. Mosteler, F.; Tukey, J. W. Addison-Wesley: Reading, MA; 1977.
56. Philippopoulos, M.; Lim, C. J Phys Chem 1994, 98, 8264–8273.
57. Philippopoulos, M.; Lim, C. J Mol Biol 1995, 255, 771–792.
58. Sunada, S.; Go, N. J Chem Phys 1996, 44, 4768–4775.
59. Bruschweiler, R.; Case, D. A. Phys Rev Lett 1994, 72, 940–943.
60. Bruschweiler, R.; Case, D. A. Proc NMR Spectrosc 1994, 26, 27–58.
61. Bruschweiler, R. J Am Chem Soc 1992, 114, 5341–5334.
62. Levy, R. M.; Karplus, M.; Wolynes, P. G. J Am Chem Soc 1981, 103, 5998–6011.
63. Olejiniczak, E. T.; Dobson, C. M.; Karplus, M.; Levy, R. M. J Am Chem Soc 1984, 106, 1923–1930.
64. London, R. E.; Avitabile, J. J Am Chem Soc 1978, 100, 7159–7165.
65. Palmer, A. G.; Case, D. A. J Am Chem Soc 1992, 114, 9059–9067.
66. Smith, P. E.; van Schaik, R. C.; Szyperski, T.; Wuthrich, K.; van Gunsteren, W. F. J Mol Biol 1995, 246, 356–365.
67. Chandrasekhar, I.; Clore, G. M.; Szabo, A.; Gronenborn, A. M.; Brooks, B. R. J Mol Biol 1992, 226, 239–250.
68. Abseher, R.; Ludemann, S.; Schreiber, H.; Steinhauser, O. J Mol Biol 1995, 249, 604–624.
69. Lee, C. S.; Kumar, T. K. S.; Lian, L. Y.; Cheng, J. W.; Yu, C. Biochemistry 1998, 37, 155–164.
70. Darden, T. A.; York, D.; Pedersen, L. J Chem Phys 1993, 98, 10089–10092.
71. Fox, T.; Kollman, P. A. Proteins 1996, 25, 315–334.
72. Schneider, D. M.; Dellwo, M. J.; Wand, A. J. Biochemistry 1992, 31, 3645–3652.
73. Quenouille, M. H. Biometrika 1956, 43, 353–360.
74. Brooks, C. L.; Karplus, M.; Pettitt, B. M. Proteins: A theoretical perspective of dynamics, structure, and thermodynamics; John Wiley & Sons: New York; 1988.
75. Pearlman, D. A.; Case, D. A.; Caldwell, J. W.; Ross, W. S.; Cheatham, T. E.; DeBolt, S.; Ferguson, D.; Seibel, G.; Kollman, P. A. AMBER 4.1; University of California, San Francisco, San Francisco, CA; 1995.
76. Berendsen, H. J. C.; Postma, J. P. M.; van Gunsteren, W. F.; DiNola, A.; Haak, J. R. J Chem Phys 1984, 81, 3684–3690.
77. Allen, M. P.; Tildesley, D. J. Computer simulation of liquids; Oxford Science Publications: Oxford, UK 1989.
78. Cornell, W. D.; Cieplak, P.; Bayly, C. I.; Gould, I. R.; Merz, K. M.; Ferguson, D. M.; Spellmeyer, D. C.; Fox, T.; Caldwell, J. W.; Kollman, P. A. J Am Chem Soc 1995, 117, 5179–5197.
79. York, D. M.; Darden, T. A.; Pedersen, L. G. J Chem Phys 1993, 9, 8345–8348.
80. Cheatham, T. E.; Miller, J.; Fox, T.; Kollman, P. A. J Am Chem Soc 1995, 117, 4193–4194.
81. Weerasinghe, S.; Smith, P. E.; Mohan, V.; Cheng, Y. K.; Pettitt, B. M. J Am Chem Soc 1995, 117, 2147–2158.

82. Kollman, P. A. Acc Chem Res 1996, 29, 461–469.
83. Cheatham, T. E.; Kollman, P. A. J Am Chem Soc 1997, 119, 4805–4825.
84. Cheatham, T. E.; Crowley, M. F.; Fox, T.; Kollman, P. A. Proc Natl Acad Sci USA 1997, 94, 9626–9630.
85. Cheatham, T. E.; Miller, J. L.; Spector, T. I.; Cieplak, P.; Kollman, P. A. ACS Symposium Series. Molecular Modeling and Structure Determination of Nucleic Acids. ACS: Washington, DC; 1997.
86. Cheatham, T. E.; Kollman, P. A. Structure, 1997, 5, 1297–1311.
87. Spector, T. I.; Cheatham, T. E.; Kollman, P. A. J Am Chem Soc 1997, 119, 7095–7104.
88. Miller, J. L.; Kollman, P. A. J Mol Biol 1997, 270, 436–450.
89. Cieplak, P.; Cheatham, T. E.; Kollman, P. A. J Am Chem Soc 1997, 119, 6722–6730.
90. Philippopoulos, M.; Mandel, A. M.; Palmer, A. G.; Lim, C. Proteins 1997, 28, 481–493.
91. Petsko, G. A.; Ringe, D. Ann Rev Biophys Bioeng 1984, 13, 331–371.
92. Dufourcq, J.; Faucon, J. F.; Bernard, E.; Pezolet, M. Toxicon 1982, 20, 165–174.
93. Batenburg, A. M.; Bougis, P. E.; Rochat, H.; Verkleij, A. J.; de Kruijff, B. Biochemistry 1985, 24, 7101–7110.
94. Bougis, P.; Rochat, H.; Pieroni, G.; Verger, R. Biochemistry 1981, 20, 4915–4920.